International Journal of Civil Engineering (2023) 21:1709–1724
https://doi.org/10.1007/s40999-023-00859-9

RESEARCH PAPER

Investigation of the Protection Efficiency of Repair Mortar Against Chloride Corrosion in Repaired Zones of Reinforced Concrete

Abderrahmane Soufi[1] · Abdelkarim Aït-Mokhtar[2] · Pierre-Yves Mahieux[2] · Amiri Ouali[3]

Received: 16 November 2022 / Revised: 21 May 2023 / Accepted: 10 June 2023 / Published online: 22 June 2023

Abstract

In this study, specimens with concrete interfaces and repair mortar were designed to simulate a concrete repair system to investigate the efficiency of seven polymer-based cement repair mortars when they were applied to concrete supports. The steel protection capacity of the mortars against chloride attack and chloride diffusion along the interface between the concrete support and the repair mortar was analysed. The mortar/concrete support system was studied using accelerated chloride corrosion tests and open-circuit potential measurements to monitor the behaviour of the steel rebar embedded in the system. The results highlight that the performance of mortar against chloride corrosion depends on its durability and mechanical properties, such as porosity, pore-size distribution, chloride diffusion coefficient, compressive strength, and bond strength. A high-polymer proportion in the mortar (polymer/cement ratio = 0.21) helps reduce chloride penetration but reduces the critical chloride concentration responsible for the initiation of corrosion. In addition, the mortar's bond strength of 0.8 MPa leads to crack development in the mortar/C30 concrete support system. A crack width of 5 μm at the interface increases the chloride diffusivity along this interface, and consequently, the risk of corrosion initiation.

Keywords Durability · Polymer modified mortar · Chloride penetration · Repair mortar · Mechanical properties · Potential corrosion

1 Introduction

Most reinforced concrete structures in OECD countries, especially marine structures, are more than 60 years old, and many of them require repairs for the damages they are facing. Corrosion is the main cause of damage and leads to disorders in the concrete and reinforcements. In marine structures, corrosion is caused by the penetration of chloride ions into porous networks of concrete covers. When the chloride concentration reaches a critical threshold, the passive layer that protects the steel reinforcement against corrosion is modified by chemical reactions that lead to the local destruction of the protective layer. When the steel is de-passivated, corrosion is initiated, thus causing cracking of the concrete cover [1–4]. Mortar patch repair is one of the most commonly used techniques for repairing damage caused by the local corrosion of reinforced concrete [5–7]. The objective of repairing reinforced concrete with mortar is to replace the defective concrete cover with repair mortar and restore the structural integrity and durability of the reinforced concrete elements. The efficiency and durability

✉ Abderrahmane Soufi
asoufi@cesi.fr

Abdelkarim Aït-Mokhtar
karim.ait-mokhtar@univ-lr.fr

Pierre-Yves Mahieux
pierre-yves.mahieux@univ-lr.fr

Amiri Ouali
ouali.amiri@univ-nantes.fr

[1] CESI LINEACT, Campus Montpellier Immeuble le Quatrième Zone Aéroportuaire de Montpellier-Méditerranée, 34130 Mauguio, France

[2] La Rochelle University, CNRS LaSIE UMR 7356, Av. Michel Crépeau, 17042 La Rochelle cedex 1, France

[3] University of Nantes, CNRS, GeM UMR 6183, Polytech Nantes, Bd de l'université, BP152, 44603 St-Nazaire cedex, France

of the system depend on the durability of the repair mortar and its ability to protect the reinforcement against corrosion, but also on the durability of the interface, which is the weakest part of the repaired system [8]. Therefore, it is important to select a suitable material for concrete repair. Polymer-based cement mortar is one of the most commonly used materials for repairing concrete. These materials include cement, sand, mineral admixtures, and polymers. Ethylene–vinyl acetate (EVA), polyacrylic ester (PAE), styrene acrylic ester (SAE), and styrene-butadiene rubber (SBR) are the most commonly used polymers [9]. Numerous studies have reported that polymers are the main effective compounds that modify the microstructure and mechanical and durability properties of mortar [10–15]. The microstructure of polymer-based cement mortar depends on the interactions between the cement matrix and polymeric phase. The types of these interactions are not yet clear and some controversies exist among researchers. Some researchers believe that only physical interactions occur between cement and polymer. Physical interactions can result in the formation of a polymeric film which is responsible for the improvement of the properties of hardened mortars [11, 12]. Other researchers believe that both physical and chemical interactions occur between polymers and cement. Chemical interactions can result in the formation of complex structures and changes in the morphology, composition, and quality of hydrated cement phases, especially calcium hydroxide [10, 12–14]. These interactions lead to a lower pH in the pore solution [15]. This could affect the passive layer that protects the reinforcement and negatively affects the ability of the repair mortar to protect the reinforcement against chloride corrosion.

Regarding the mechanical properties, previous studies have shown that polymer-based cement mortars show improvements in tensile and flexural strengths with an increased polymer-to-cement ratio (*P*/*C*), but yield a reduced compressive strength [11, 14, 16]. Some researchers have associated the increase in tensile and flexural strengths with film formation, reduction in microcracks in the cement matrix, and improvement in the adhesion between aggregates and cement. In contrast, some researchers have attributed the decrease in compressive strength to different phenomena, such as increased porosity due to the air-entrainment effect of polymer surfactants, delay in the cement hydration process, reduction of elastic modulus, and polymer–cement chemical reactions that create less stiff hydrate structures when subjected to compression. Regarding the pore structure, the air-entrainment effect of the polymer contributes to an increase in the total porosity and a decrease in open pores, especially in high-polymer proportion cases [12]. However, the total porosity can be reduced using an appropriate polymer dosage. According to some studies, polymers contribute to pore refinement owing to their pore-filling effects [17]. Nevertheless, some studies have reported an increase in the threshold pore size due to the presence of polymers [18–20].

The addition of the polymer also influenced the penetration of chloride into the mortar. According to Aggarwal et al. [21], the addition of an acrylic polymer with a *P*/*C* ratio of 20% reduced the depth of chloride penetration by 40% in immersion tests. Saija [22] also reported a decrease in the penetration depth with increases in the *P*/*C* ratio for a mortar modified with an acrylic polymer. Zhong et al. [23] measured the diffusion coefficient of two mortars modified by SBR SAE polymers with a *P*/*C* ratio of 10% and obtained a decreased coefficient value. Gao et al. [24] studied the influence of the *P*/*C* ratio and silica fume on the effective diffusion coefficient of the PAE type. The results showed a decrease in the effective diffusion coefficient of chlorides at increasing *P*/*C* ratios. Yang et al. [25] obtained similar results for SBR polymers. These results can be explained by the formation of a polymer film and an increase in the ability of the polymer to bind chlorides.

Based on the studies mentioned above, polymers can improve tensile and flexural strengths, pore size, and chloride diffusion; however, they have some disadvantages, such as increased total porosity, decreased compressive strength, and reduced pore solution pH. Despite the existence of numerous studies on this topic, a comprehensive understanding of the effects of polymers on durable concrete repair is lacking. Therefore, difficulties remain in the selection of appropriate repair mortars, particularly in chloride-contaminated environments. The mechanical and durability characterisation of repair mortars alone is insufficient to predict the steel protection capacity of polymer-based cement mortars. There are almost no studies available on chloride-induced corrosion and the chloride threshold level for corrosion when repair materials have already been applied to concrete, that is, in repaired structures.

Several studies have investigated the bonding behaviour of concrete interfaces [26–30]. However, the durability of these interfaces has rarely been investigated [8].

To fill this knowledge gap, specimens with concrete–repair mortar interfaces were designed to emulate a concrete repair system to investigate the efficiency of six repair mortars when applied to concrete supports. Chloride diffusion and chloride-induced corrosion were investigated. The durability parameters of materials, such as chloride diffusion (in mortars and mortar/concrete interface), pore-size distribution, and porosity of mortars and concrete supports, were studied. The protective ability of the repair materials for steel rebar was studied experimentally based

on an accelerated chloride corrosion test on reinforced concrete systems repaired using these mortars.

2 Experimental Program

2.1 Materials and Specimen Preparation

Seven repair mortars complying with the EN1504 standard [31] and modified with a polymer (ethyl acrylate-styrene-acrylamide) were used to prepare the specimens. The concrete used as a support in this study (C30) contained blended cement CEM II/A-LL 32.5 (complying with the EN 197-1 standard) from Lafarge-Holcim (France). Its chemical composition is listed in Table 1. The concrete strength class was C30/35 according to EN 206-1 [32]. The class of sand used was 0/4 mm with a density of 2480 kg/m^3. The class of the coarse aggregate was 6/10 mm with a density of 2970 kg/m^3. Table 2 lists the mix proportions of the materials (mortar and concrete).

Cylindrical specimens (diameter = 110 mm and height = 220 mm) of mortar, concrete, and mortar–concrete interfaces (half mortar and half concrete in the longitudinal direction) were prepared for mechanical and durability characterisation. Cylindrical samples with a mortar-concrete interface (Fig. 1) were cast to study the chloride diffusivity at the mortar/concrete interface. A silicone part was used to ensure equivalent roughness at the interface for all specimens. The manufacturing steps are as follows:

Stage 1: Manufacturing of silicone borrower. Silicone was cast in a cardboard mould containing half-cylindrical concrete to obtain a rough surface.

Stage 2: Casting concrete in a mould using a vibrating table and curing for 24 h in a conditioned room (20 °C and 95% relative humidity (RH)).

Stage 3: Casting mortar in a mould containing half-hardened concrete.

Stage 4: Manufacture disc samples (diameter = 70 mm and thickness = 20 mm). The resin was laterally applied to ensure unidirectional migration.

To simulate a repair system (reinforced concrete repaired with mortar), 200 mm × 200 × 55 mm^3 were manufactured for corrosion tests and coded MR1–MR7 (according to the type of repair mortar used). These samples were prepared using patch mortars (MR1 to 7) as a cover material in the repair system (thickness = 20 mm) and C30 concrete as a support material (thickness = 35 mm). The 20 mm cover was chosen as it corresponds to the minimum durability cover for exposure class XS according to standard 206–1. Prior to embedding them centrally in the specimen, steel rebars of 8 mm in

Table 2 Mix proportions of the materials (mortars and concrete used as a support material. W/C ratios are based on manufacturer instructions)

Mortars	*P/C*	W/C	L/C	S/C
MR1	0.06	0.48	0.05	0.96
MR2	0.05	0.43	0.05	1.60
MR3	0.04	0.35	0.16	1.48
MR4	0.07	0.43	0.07	1.58
MR5	0,08	0.50	0.15	2.13
MR6	0.07	0.51	0.20	2.74
MR7	0.21	0.19	0.02	0.80
Concrete	Gravel (kg/m^3)	Sand (kg/m^3)	Cement (kg/m^3)	Water (kg/m^3)
	1205	593	380	193

C: cement, P: Polymer, W: water, L: limestone, S: sand

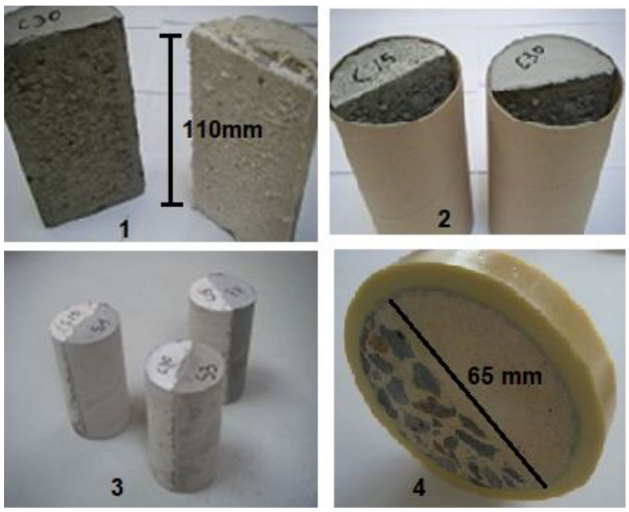

Fig. 1 Manufacturing process of mixed cylindrical samples with mortar–concrete interface

Table 1 Chemical composition of the cement used (wt%)

SiO_2	Al_2O_3	Fe_2O_3	CaO	MgO	SO_3	K_2O	Na_2O	Loss of ignition
20.40	4.07	2.87	60.31	1.25	3.15	1.31	0.13	6.51

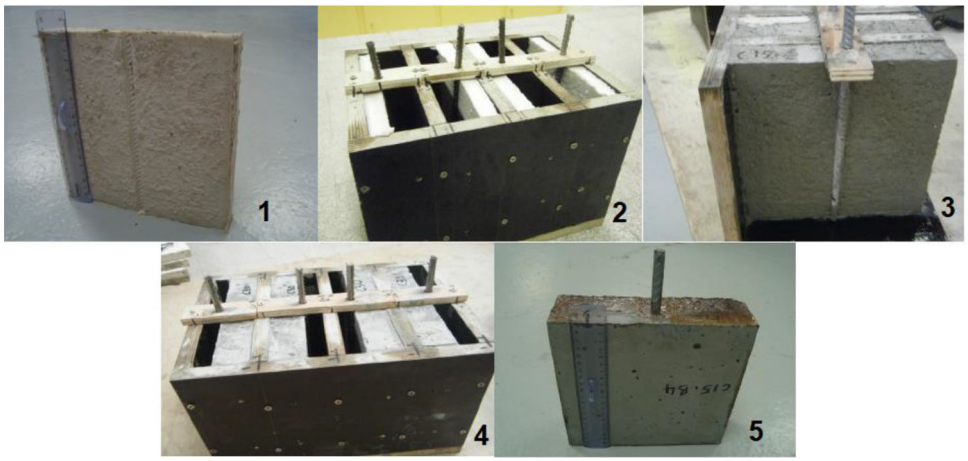

Fig. 2 Manufacturing process of reinforced concrete sample repaired with a mortar

diameter and 24 cm in length were cleaned using electric brushing. A silicone part with a rough surface was used to obtain an equivalent rough surface for proper bonding between concrete and mortar. The manufacturing process of the system is described as follows (Fig. 2):

Stage 1: Manufacturing of silicon borrowing. The silicone was cast in a mould which contained a test piece of sandblasted prismatic concrete on which reinforcement was glued to obtain a silicone piece with the impression of reinforcement and sandblasted concrete.

Stage 2: Placement of borrow pits and reinforcement before casting the concrete into three layers by vibration and conservation of the mould in a wet chamber for 24 h. The reinforcement steel was kept straight using a wooden cleat attached to the mould. The apparent part of the steel reinforcement was galvanised in stage 5.

Stage 3: Casting concrete, curing for 24 h in a conditioned chamber (20 °C and 95%RH), and releasing borrows from the mould.

Stage 4: Mortar casting in three layers using vibration in a mould containing half concrete and reinforcement.

Stage 5: Release samples from the mould, galvanisation of the apparent part of the steel reinforcement, and conservation in a conditioned chamber for 28 days (d) (20 °C and 95%RH). A schematic of the manufactured sample is shown in Fig. 3.

2.2 Mechanical Properties of Materials

The compressive strength, flexural strength, and modulus of elasticity of the mortars were measured on prismatic specimens (40 × 40 × 160 mm) according to the standards EN 12190 and EN 13412 [33–35]. The specimens were de-moulded 24 h after casting and packed in a plastic film for 48 h. They were then placed in a conditioned chamber for 28 days. The bond strengths of the mortars

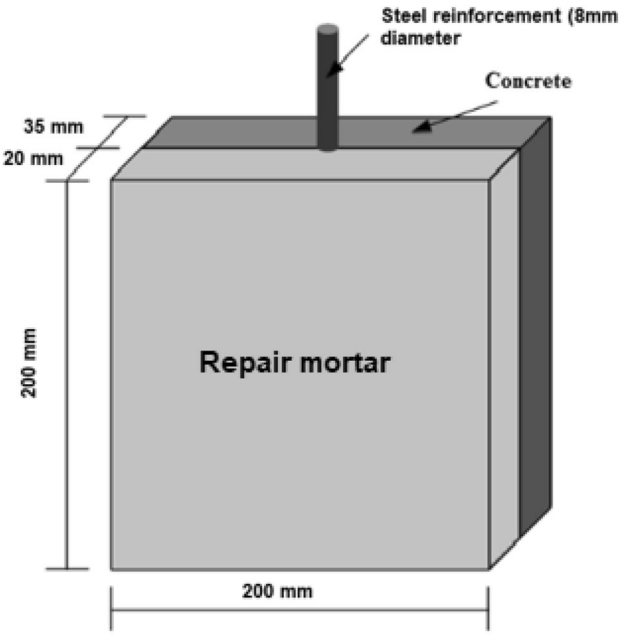

Fig. 3 Reinforced concrete sample repaired with a mortar

were determined using the EN 1542 standard [36]. The mechanical properties of the concrete were determined

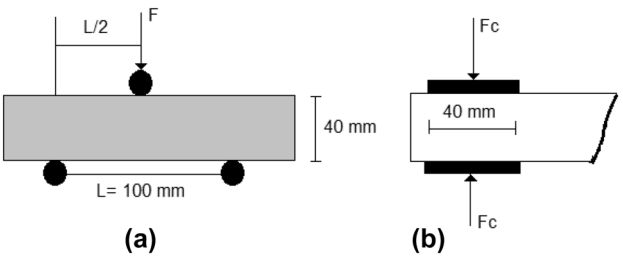

Fig. 4 Schematics showing three points bending (**a**) and compression (**b**) tests for repair mortars

according to the NF EN 12390-3, 12390-6, and 12390-13 standards [37–39].

The compressive strength, modulus of elasticity in compression, and flexural strength of the mortars were measured using prismatic specimens with dimensions of 40 mm × 40 mm × 160 mm. The specimens were demoulded after 24 h and wrapped in plastic film for 48 h. They were then unwrapped and cured for 25 days in a laboratory. Compression and three-point bending tests were conducted on each mortar sample (see Fig. 4). The elasticity modulus of the repair mortar was measured by applying an axial compressive load to the specimen and relating the longitudinal compressive strain to the compressive stress. The secant modulus was established by measuring the change in the strain in the specimen when loaded to produce a stress value which ranged from 0.5 MPa to one-third of the compressive strength of the specimen. Pull-off bond tests were conducted on concrete test specimens prepared with a grit-blasted surface. Repair mortar was applied to the grit-blasted surfaces of the reference concrete specimens. The test method involved direct dolly pull-off tests using a dolly bonded to the surface of the repair system, with the test area defined by coring through the surface. A partial core was drilled perpendicular to the surface of the repair mortar and extended beyond the interface to the concrete support. Subsequently, a dolly was attached to the surface and a tensile force was applied until failure occurred (see Fig. 5). The compressive strength, modulus of elasticity in compression, and tensile strength of the concrete were measured using cylindrical specimens (diameter = 110 mm and height = 220 mm). For the compression tests, the specimens were loaded to failure using a compression testing machine. The maximum load sustained by the specimen was recorded and the compressive strength of the concrete was calculated. In the tensile test, the specimen was subjected to a compressive force applied along its length. The resulting tensile force caused the concrete specimens to fail when subjected to tension (see Fig. 6). To determine the modulus of elasticity, a test specimen was loaded (axial compression), the stresses and strains were recorded, and the slope of the secant to the stress–strain curve was determined at the first loading.

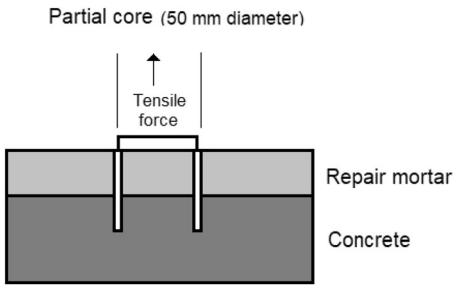

Fig. 5 Schematic of a pull-off test

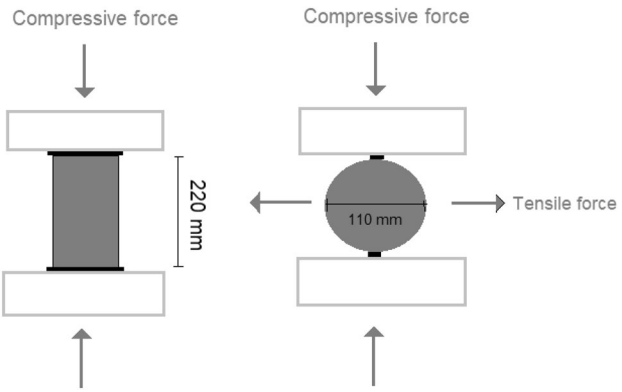

Fig. 6 Schematics of compression and tensile tests for concrete

2.3 Porosity and Chloride Diffusivity

Water porosity was measured on three cylinders (diameters = 65 mm and thicknesses = 15 mm) for each material according to the procedure recommended by Grandubé [40]. Mercury intrusion porosimetry (MIP) was performed using a micromeritics porosimeter (Autopore III 9420). Its pressure limit reached 420 MPa, which corresponded to pores with approximate diameters equal to 3 nm according to the Laplace–Washburn law [41].

The chloride diffusion coefficients of the materials (mortars, concrete, and mixed mortar–concrete samples) were assessed by a migration test at steady state on cylindrical samples (diameters = 65 mm and thicknesses = 15 mm) cored and saw-cut from cylindrical specimens with dimensions of 110 × 220 mm [3–5]. Before the migration tests, the samples were saturated with a basic solution composed of 25 mM NaOH and 83 mM KOH. This basic solution was also used in the two-cell compartments, and NaCl (0.5 M) was added to the upstream compartment. An electric field applied between the two sides of the sample was 300 $V.m^{-1}$. The curve of the cumulative concentration of chlorides in the downstream compartment was plotted against time. The slope of the curve ($\frac{\Delta C}{\Delta t}$) was determined, and the flow was calculated using the following relationship:

$$J = \frac{\Delta C}{\Delta t}\frac{V}{S}\left(\text{mol. M}^{-2}.\text{s}^{-1}\right) \quad (1)$$

where V (l) is the volume of the downstream compartment, S (m^2) is the section of the sample, and ΔC is the increase in the chloride concentration downstream (mol) during the time interval Δt (s). The effective chloride diffusion coefficient (D_{eff}) was calculated using the following relationship [3]:

$$D_{eff} = \frac{RTJ}{ZFEC_0}\left(1 - e^{\frac{ZFU}{RT}}\right)\left(m^2.s.^{-1}\right) \quad (2)$$

where R is the constant of an ideal gas (8.32 J.mol^{-1}.K^{-1}), T is the temperature (kelvin, C_0 is the chloride concentration in the upstream compartment (mol.m^{-3}), F is the Faraday constant (96,487 C.mol^{-1}), E is the applied electrical field (300 V.m^{-1}), and U the corresponding potential difference (V).

The theoretical diffusion coefficient of the mixed mortar-concrete samples with an interface was determined by averaging the coefficients of the mortar and concrete, as half of the cross-section of the exposed sample was the mortar and the other half was concrete.

2.4 Chloride Accelerated Corrosion Test

Figure 7 shows a chloride-accelerated corrosion cell. The sample was placed between two compartments which contained a basic and saline solution. Polarisation was performed using two stainless-steel plates. During the test, the chloride migration under the electrical field of 50 V.m^{-1} and open-circuit potential measurements were conducted. The value of 50 V.m^{-1} was chosen to monitor the corrosion potential of the rebar during chloride migration. Migration and potential measurements were performed every 2 h until the potential became more negative than − 276 mV vs. the saturated calomel electrode. Tests were performed on repair systems of 200 mm × 200 × 55 mm^3 saturated with a basic solution of NaOH and KOH for diffusivity measurements, as stated above [1]. At the end of this test, the chloride concentrations were determined over the entire thickness of the coating and up to the steel reinforcement.

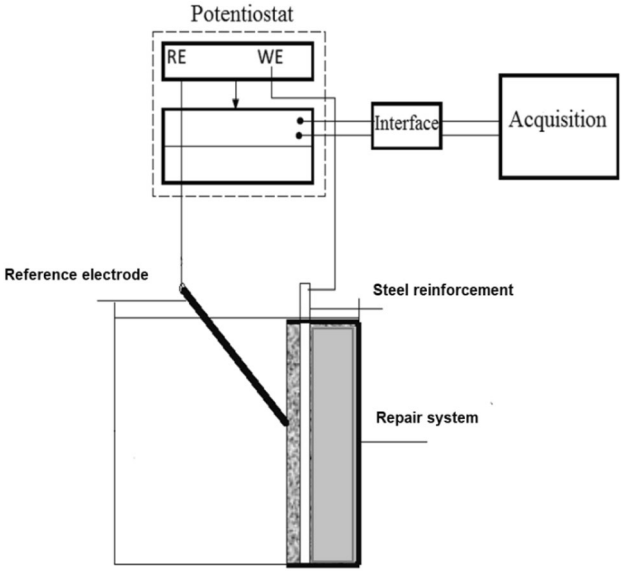

Fig. 8 Schematic representation of the open-circuit potential (OCP) measurement setup

2.5 Open-Circuit Potential (OCP) Measurements/ Corrosion Monitoring

We measured the corrosion potential of the rebar with a saturated calomel electrode (SCE) according to the American standard ASTM 876 [42]. The purpose of this test was to measure the potential difference between the reference electrode and the steel reinforcement (see Fig. 8).

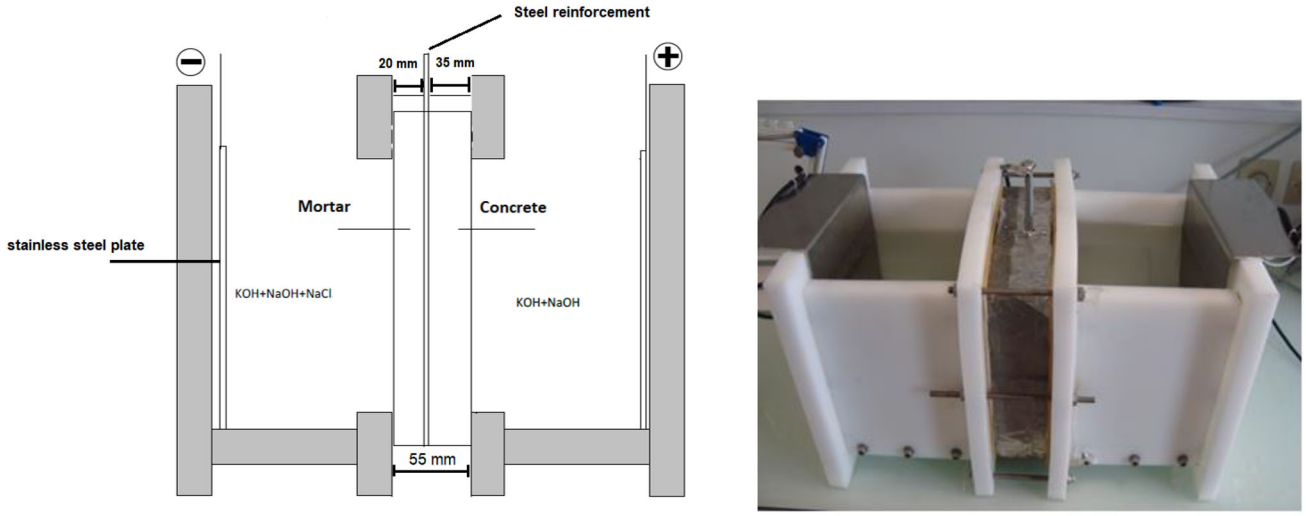

Fig. 7 Schematic and photograph of chloride-accelerated corrosion cell

The steel reinforcements and electrodes were connected to a potentiostat (Solarton 1285). According to this standard, when the potential of steel in the system becomes more negative than − 276 mV vs. saturated calomel electrode, it means that there is a 90% probability that corrosion will occur. Note that this method can provide information about the corrosion probability, but cannot indicate the rate of corrosion.

2.6 Determination of Total and Free Chloride and Scanning Electron Microscopy (SEM) Analyses

After the OPC measurements were completed, powder samples for chloride dosages were drilled perpendicular to all the specimen faces at various depths. Each specimen was drilled using a rotary percussion drill at the depths of 2, 4, 6, 8, 10, 12, 14, 16, 18, and 20 mm from the surface exposed to chlorides. Drilling was performed from the sample's surface to the penetration depth of the chloride ions in the mortars. Extraction of total and free chlorides from the powder was performed according to Grandubé's recommendations [40]. SEM was used to analyse the mortar/concrete interface. A Quanta 200 microscope (Philips ESEM/FEG) was used.

3 Results and Discussion

3.1 Mechanical Properties

As shown in Table 3, MR5 mortar exhibited the lowest compressive and bond strengths, whereas MR3 exhibited the highest values. The flexural strength of MR7 was higher than those of the other mortars. However, reductions in the compressive strength of 11 to 22% were observed with respect to the MR2, MR3, and MR4 mortars (PC ratios in the range of 4–7%). As already discussed, the improvement in flexural strength is due to the higher polymer proportion (*P*/*C* ratio of 19%) that increases the adhesion strength between the aggregate and the binder [9]. The loss in compressive strength was due to an increase in porosity caused by the air-entraining effect of the polymer. The correlation between the flexural and compressive strengths was investigated and compared with previous studies. Medeiros et al. [43] and Kim et al. [9] reported a good relationship between the two strength values with R^2 values of 0.9 and 0.77, respectively. In this study, we found a poor relationship between the two strength values (R^2 = 0.13) (see Fig. 9).

The correlation between the compressive and bond strengths of the mortars was analysed, as illustrated in Fig. 10. A strong relationship exists between the two mechanical properties, with an R^2 value of 0.84. This result is inconsistent with that reported by Medeiros et al. [43]. Kim et al. [9] found a poor relationship (R^2 = 0.24).

Table 3 Mechanical properties of mortars and concrete support with their respective standard deviations

Material	Compressive strengths 28 days (MPa)	Flexural strengths 28 days (MPa)	Bond strength by the pull of 28 days (MPa)	Modulus of elasticity in compression (GPa)
MR1	44 ± 3	5.8 ± 0.8	1.7	19.4
MR2	65 ± 2	7.6 ± 0.5	2.5	24.8
MR3	68 ± 4	8.1 ± 1	2.5	29.9
MR4	60 ± 2	8.8 ± 0.7	2.4	20.1
MR5	41 ± 1	7.2 ± 0.5	0.8	20
MR6	48 ± 1.5	8.2 ± 0.6	1.5	22.6
MR7	53 ± 4	10.2 ± 0.7	2.1	21.3
C30	32 ± 2	–	2.1 (tensile)	24.3

3.2 Porosity and Pore-Size Distribution of Materials

The results of the water and mercury porosities are presented in Fig. 11 for all materials. The water and mercury porosity values of the mortars were higher than those of the concrete supports. Mercury porosity values of the mortars ranged from 12 to 24%, whereas water porosity values ranged from 14 to 27%. MR3 mortar exhibited the lowest value compared with the other mortars, while MR1 mortar exhibited the highest value. The porosity of the MR1 mortar remained high compared with that of the other mortars, which may be explained by its high W/C ratio and

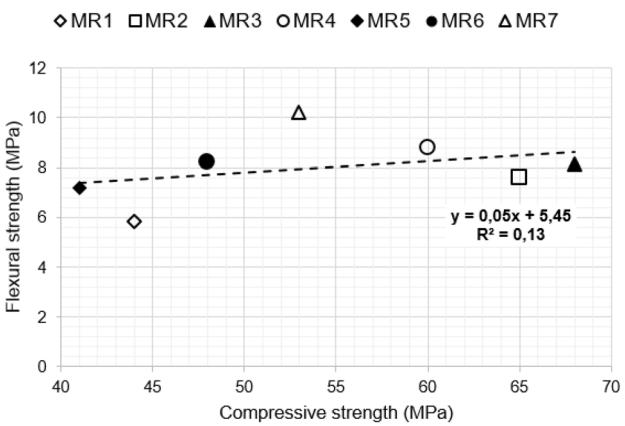

Fig. 9 Relationship between compressive and flexural strengths at 28 days

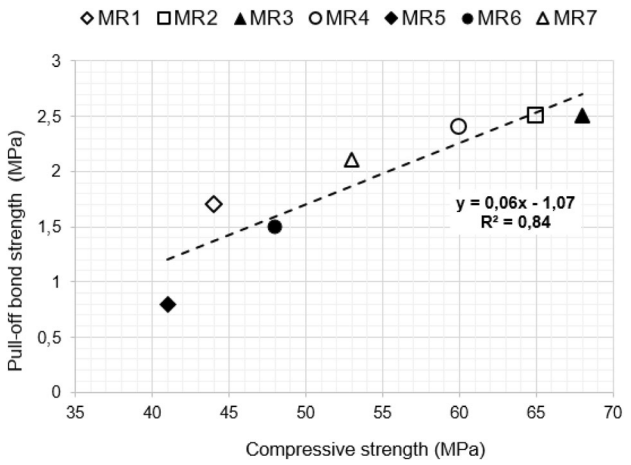

Fig. 10 Relationship between compressive and pull-off bond strengths at 28 days

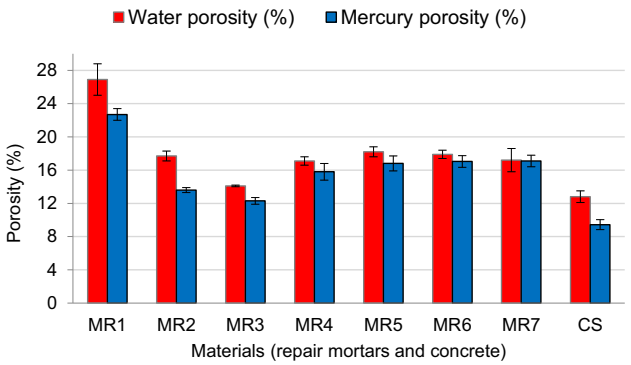

Fig. 11 Water and mercury porosities (in %) of mortars and concrete support and respective standard deviations

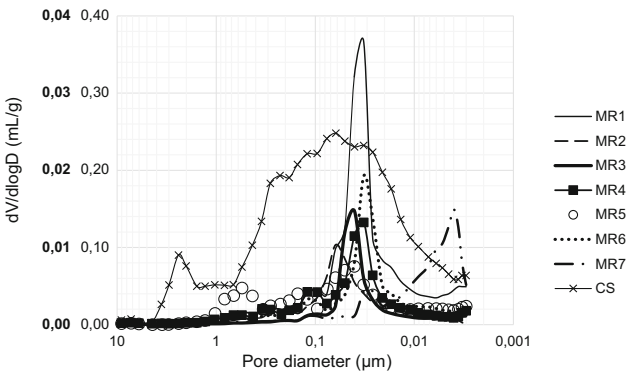

Fig. 12 Pore-size distributions of mortars and concrete support

low S/C ratio. Despite its low-W/C ratio (equal to 0.19), MR7 mortar had a fairly high porosity (value of 17.2%). These results are in agreement with the findings of other studies on acrylate polymer [15, 44, 45]. According to the authors, the increase in porosity, particularly for *P*/*C* ratios greater than 0.10, was due to the air-entrainment effect of the polymer.

Figure 12 shows the pore-size distributions of the mortar and concrete. The pore-size distribution curve of MR7 mortar, which had the lowest W/C ratio, exhibited finer pores than those of the other mortars. The main (or critical) pore diameter in the MR7 mortar was approximately 4 nm, which corresponded to hydrated pores. This critical pore diameter was in the range of 32–50 nm in the cases of the MR1–MR6 mortars, which correspond to medium capillary pores. The pore-size distribution curve of the MR7 mortar exhibited two peaks (bimodal distribution). The first was at a diameter of 4 nm, whereas the second corresponded to a diameter of ∼ 26 nm. The curves of the MR4 and MR6 mortars also exhibited two peaks: the first and largest were approximately 95 nm in diameter, and the second was at 32 nm. The MR1, MR2, and MR3 mortars exhibited one peak (monomodal distribution) with diameters in the range of 40–50 nm. The pore-size distribution curve of MR5 exhibited coarser pores and three peaks. The first had a diameter of 32 nm, whereas the second had a diameter of 150 nm. For this mortar, a third peak appeared in the diameter range of 550 nm and corresponded to large capillaries. This microstructure could be related to the higher W/C ratio (0.51) which increased the number of capillary pores [46]. Despite its lower porosity compared with those of the mortars, concrete support (CS) presents a coarser pore-size distribution. On the y-axis, values from 0 to 0.04 are those of the mortar, and values from 0 to 0.4 are those of concrete. The pore-size distribution curve of MR7 mortar, which had the lowest W/C and highest *P*/*C* ratios, exhibited finer pores than those of the other mortars. The main (or critical) pore diameter in the MR7 mortar was approximately 4 nm and corresponded to hydrated pores. This result shows that a high proportion of polymer (*P*/*C* = 0.21) induced pore-size refinement (pore diameter in the range of 4 nm). These results are in good agreement

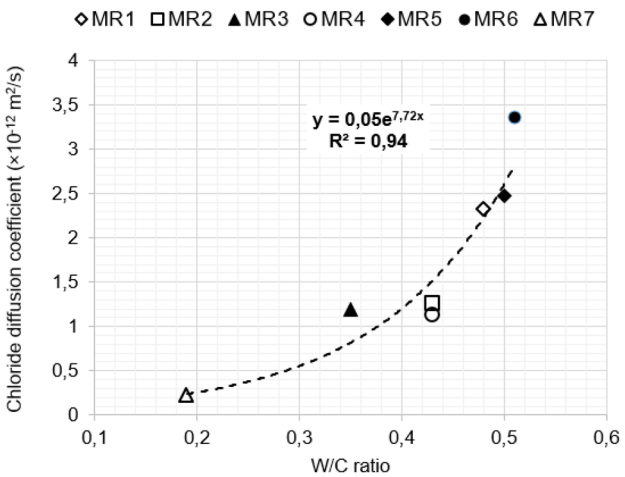

Fig. 13 Relationship between chloride diffusion coefficient and W/C ratio of repair mortars tested

with those of previous studies using acrylate polymer [15, 44, 45]. Pore refinement was due to the pore-filling effect of the polymer particles.

3.3 Chloride Diffusivity in Mortars and Mortar/Concrete Interface

The chloride diffusion coefficients as a function of the W/C ratio are shown in Fig. 13. Mortar MR7 exhibited the lowest diffusion coefficient, which was one order of magnitude lower than those of the other materials. The MR6 mortar exhibited the highest chloride diffusion coefficient. The MR2, MR3, and MR4 mortars yielded similar chloride diffusion coefficients. MR1, MR5, and the concrete support exhibited similar values. The chloride diffusion coefficient of the repair mortar was influenced by the W/C ratio. When the W/C ratio was approximately 0.2, the diffusion coefficient has an order of magnitude of 10^{-13} $m^2.s^{-1}$. When the W/C ratio ranged between 0.36 and 0.43, the diffusion coefficient values were between 1 and 1.5 × 10^{-12} $m^2.s^{-1}$. At a W/C ratio of 0.48, the diffusion coefficient doubled. These results can be explained by the effect of the W/C ratio on the porous networks of the mortars. An increase in the W/C ratio contributed to an increase in the pore size and interconnections of the porous network. Regarding the influence of the *P*/*C* ratio, values of a *P*/*C* ratio greater than 20% contribute to the deceleration of the chloride diffusion process [5]. However, in the case of values in the range of 4–8%, the chloride diffusion seems to depend on the *P*/*C* and W/C ratios. We deduced that polymer-modified mortars with low-W/C (approximately 0.2) and high- *P*/*C* ratios (approximately 20%) should have a higher resistance against chloride ion penetration. The results exhibited an abrupt decrease (an order of magnitude lower than that of other mortars) in the effective diffusion coefficient of chlorides with an increase in the *P*/*C* ratio up to 21%. This result is in good agreement with previous studies that used SBR, SAE, and PAE polymers [21–25]. This was due to pore refinement and a decrease in the number of interconnected pores.

The results of the chloride diffusion at the mortar/concrete interface are shown in Fig. 14. The theoretical diffusion coefficients of the mixed mortar-concrete samples at the interface were determined using Eq. 3. As the chloride penetration cross-section is identical for both materials, this represents the average of the diffusion coefficients of each material, determined previously (Eq. 2):

$$D_{theoretical} = \frac{D_{Concrete} + D_{Mortar}}{2} \quad (3)$$

where $D_{\text{theoretical}}$ is the theoretical chloride diffusion of the mixed mortar–concrete sample, D_{concrete} is the chloride diffusion of concrete determined using Eq. 2, and D_{mortar} is the chloride diffusion of repair mortar determined using Eq. 2 (Sect. 2.3).

The results highlight that the theoretical and experimental results were quite close for all mortars except MR5. These similarities suggest that chloride diffusion occurred only through concrete and mortar. MR5 mortar yielded a difference between theoretical (2.2 × 10^{-12} $m^2.s^{-1}$) and experimental results (5.56 × 10^{-12} $m^2.s^{-1}$). This difference suggests that chloride diffusion took place in concrete, mortar, and also at the interface area between the two materials. Cracks at the MR5/concrete interface, as observed by the SEM analysis, explain the differences between the experimental and theoretical results. The discs were cut using a circular saw. The sample to be analysed was polished, and the interface area was identified using an optical microscope and adhesive tape (see Fig. 15). The SEM images highlight cracks with a width of 0.005 mm (Fig. 16). This value was higher than the pore diameters of the concrete and MR5 mortars. Therefore, these cracks are preferential paths for chloride transport. The SEM analyses of the other mortars did not show any cracks, as shown in some examples in Fig. 17. A crack width of 5 µm at the interface affects chloride diffusion along the interface. In their study, Li et al. [8] found that crack widths between 0.08 and 0.11 mm at the interface posed no significant impact on the chloride diffusion along the interface.

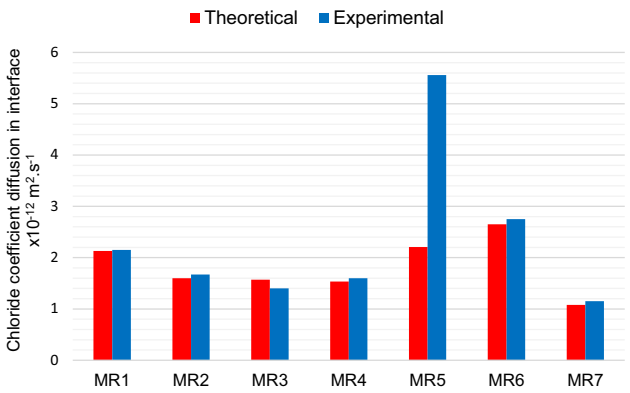

Fig. 14 Theoretical and experimental chloride diffusion coefficients of the mixing system mortar/concrete

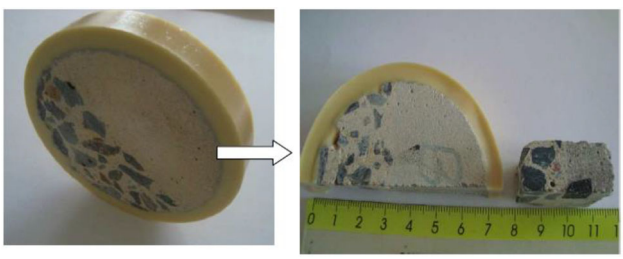

Fig. 15 Sample preparation for interface scanning electron microscopy (SEM) analysis

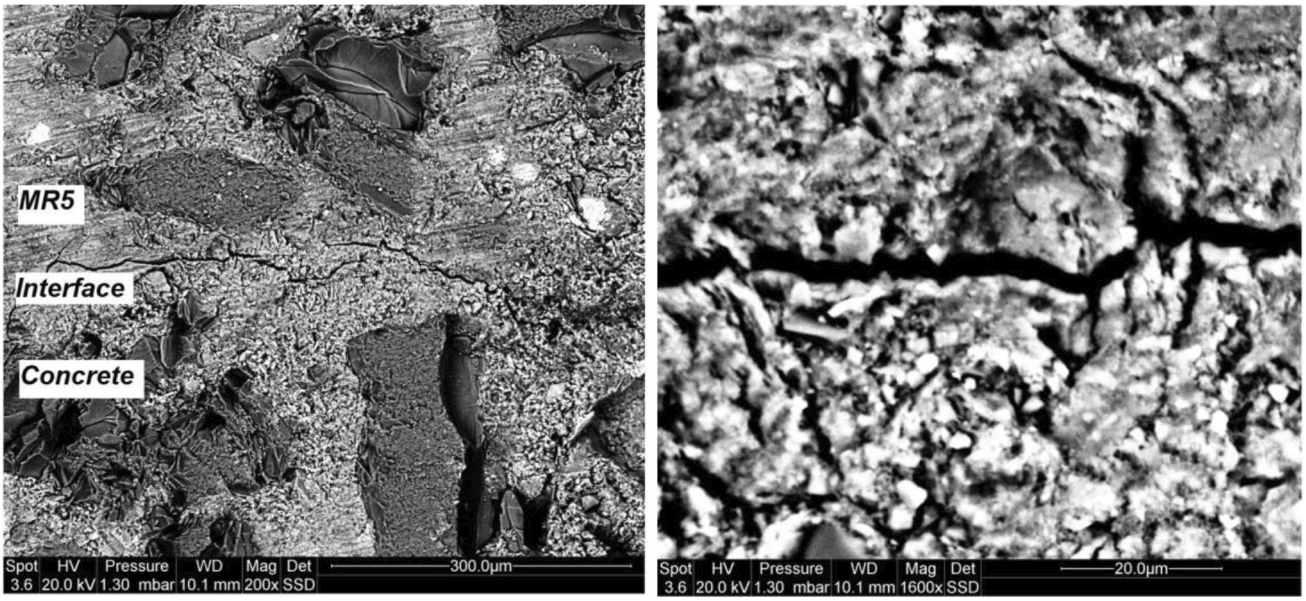

Fig. 16 SEM images of mixed mortar–concrete sample MR5 showing cracks at the interface (magnified views at 200× (left) and 1600× (right))

3.4 OCP vs. Chloride Exposure Duration

The time evolution of embedded steel potentials measured vs. SCE for different repair systems is shown in Fig. 18. The potential decreases with increasing exposure time. This decrease was attributed to the progressive increase in the chloride concentration near the steel surface. The initial potential before exposure to chlorides was between 150 and 200 mV, thus confirming that the steel was passivated [47, 48]. During the test, chloride migration shifted the potential in the negative direction. Among the samples studied, MR7 performed better than the other mortar types. Its initial potential was more than − 275 mV for exposures within 100 h. MR3 presented a similar behaviour to MR4 with an initial potential greater than − 275 mV for exposures within 50 h. MR1 and MR2 exhibited initial potentials greater than − 275 mV for exposures within 46 and 80 h. This indicates that the MR7 mortar is a better physical barrier against the corrosion of the reinforcements.

In their study, Aattache and Soltane [49] used the same corrosion monitoring method to compare the performance of mortars with *P*/*C* ratios equal to 5, 10, and 15%. They found that the mortar with a *P*/*C* ratio of 10% yielded the best performance. The samples were only composed of mortar, and cyclic wetting and drying processes were applied to accelerate the diffusion of chlorides.

Figure 19 shows the relationship between the total chloride exposure time (the time required to reach a potential of − 275 mV) and the chloride diffusion coefficient of the mortars. The exposure time decreased with an increase in the chloride diffusion coefficient. The higher the chloride diffusion coefficient of the mortar, the lower the exposure time and the higher the risk of corrosion will be. MR5 was the least efficient with a potential > − 275 mV for exposures within only 8 h. This is because of its poor adhesion to concrete supports. Indeed, the MR5 mortar had the lowest bond strength compared with the other mortars (see Table 3). Its value was 0.8 MPa, which was 1.5 to 3 times lower than those of other materials. This poor adhesion led to the development of cracks in the system and increased chloride diffusivity, and increased the risk of corrosion initiation. According to some authors [50, 51], the repair material must display an elasticity modulus similar to that of the concrete substrate to minimise cracking. In our study, there was no relationship between the modulus of elasticity and cracking owing to the type of conservation of specimens that avoided high-material shrinkage.

3.5 Profiles of Chloride Concentration in Repair Mortars

After the OCP measurements, the total and free chloride concentrations were determined via chemical analyses. The results are shown in Figs. 20 and 21, respectively. The concentration–depth curves can be divided into two parts. There is an increasing part between 2 and 4 mm and a decreasing part between 4 and 20 mm. This increase was due to the mortar skin, which was the zone closest to the surface of the system's cover. This skin effect was due to the contact of the mortar with the moulds, which produced an irregular chloride profile near the surface. In the second part of the profile, the chloride concentration decreased as a function of the depth of the sample, as is usually observed

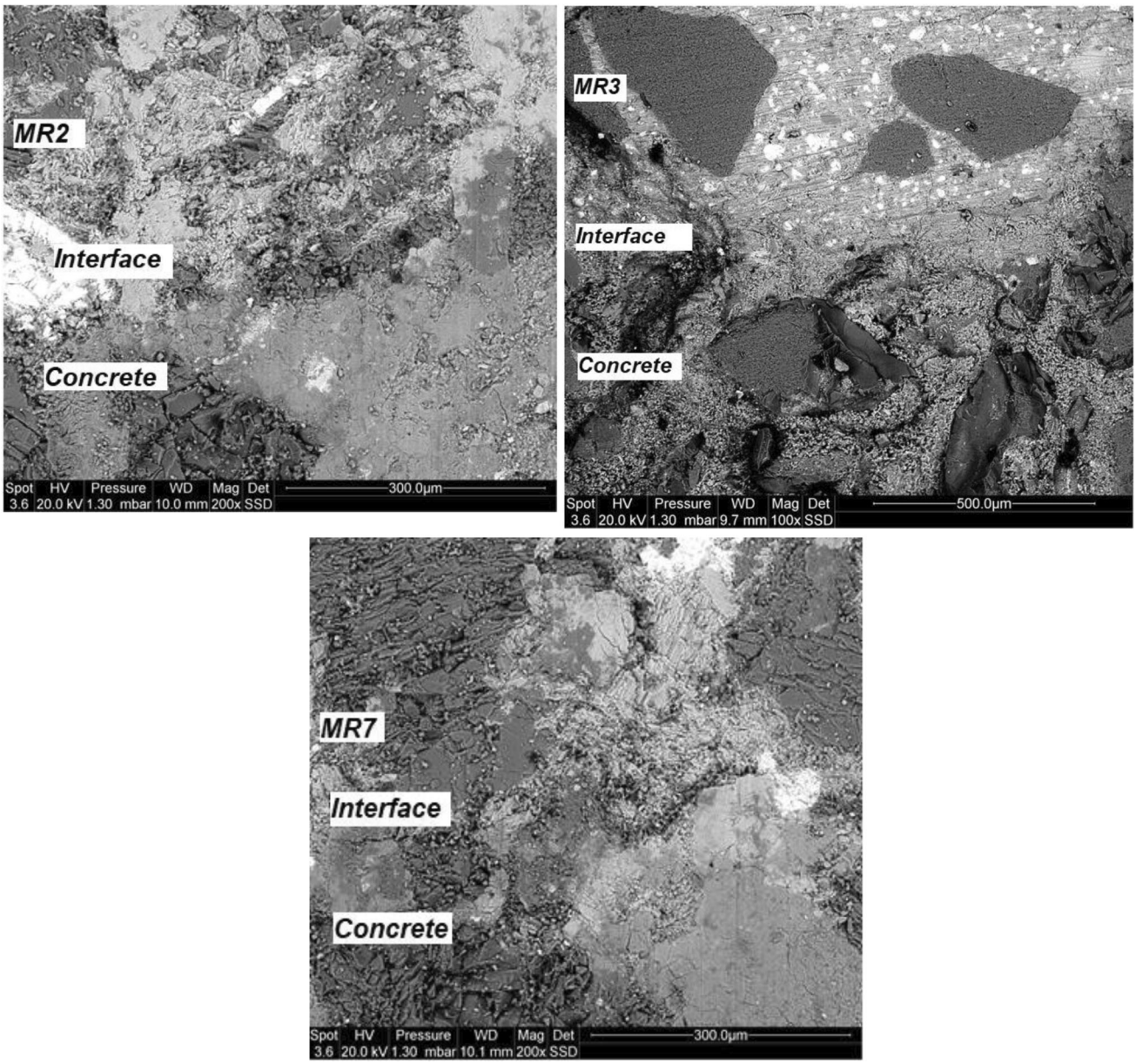

Fig. 17 SEM images of mixed mortar–concrete samples MR2, MR3, and MR7

in the literature. The results show that the chloride diffusion coefficient of the mortars (determined in the stationary regime) is not the only parameter that characterises chloride penetration in the materials. For example, MR3 and MR4 have similar chloride diffusion coefficients (1.2×10^{-12} m^2/s and 1.13×10^{-12} m^2/s, respectively) and the same exposure time, but the chloride profile of MR3 is different from that of MR4. The chloride profile of MR3 was relatively flat and showed a small increase in the chloride concentration at all depths. In contrast, the profile of MR4 is steeper at depths in the range from 4 to 12 mm. These results suggest that despite the similar effective diffusion coefficients of the two mortars, the porous network was not the same over the entire thickness of the coating.

It is noted that total chloride concentration values at a depth of 20 mm lie between 0.044 and 0.07% of the mass of the mortar, whereas the free chlorides vary between 0.04 and 0.059%. The difference in free chloride concentration is linked to some parameters, mainly the state of the steel–mortar interface, concentration of the ion hydroxyls (pH), surface quality of steel, and the potential of steel [52–54]. For our samples, the parameters which can be considered when comparing the chloride concentrations are the state of the interface and the pH. Indeed, according to the potential measurements, all the samples had almost the same

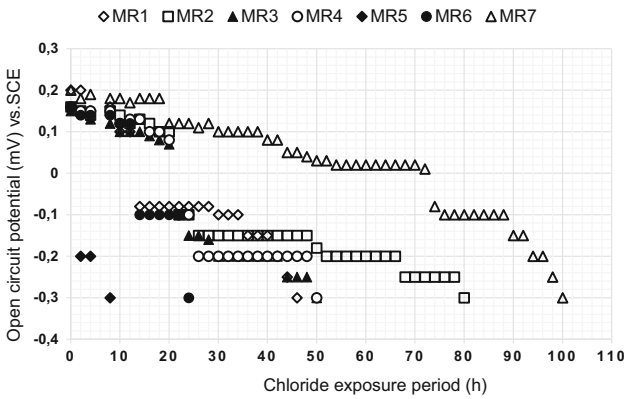

Fig. 18 Plots of OCP vs. chloride exposure time in repair systems (MR1 to MR7)

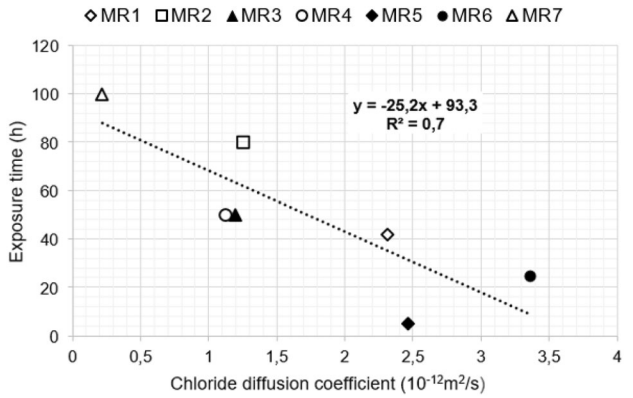

Fig. 19 Relationship between the exposure time of repair systems (required to reach an OCP of − 275 mv) and chloride diffusion coefficient of mortars

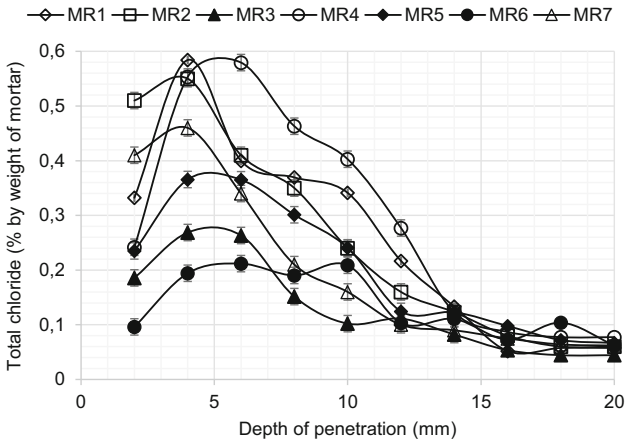

Fig. 20 Total chloride profiles in repair mortars cast as a coating at the end of OPC measurements

potential before the initiation of corrosion. Regarding the surface quality of the steel, the reinforcements were subjected to the same electric brushing treatment prior to casting the specimens. Therefore, the potential and steel

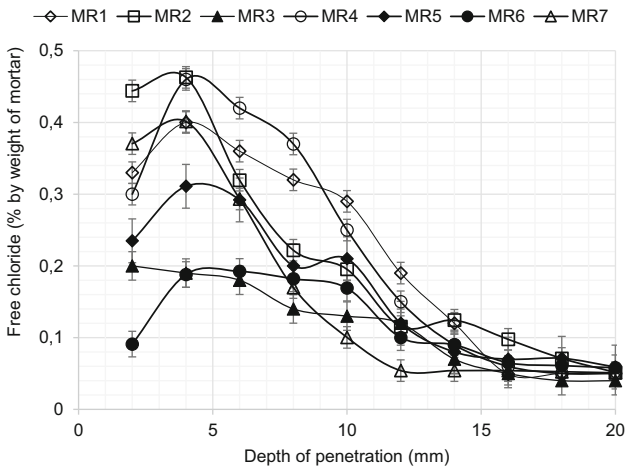

Fig. 21 Free chloride profiles in repair mortars cast as coatings

surfaces could be excluded. Concerning pH, some researchers consider that the molar ratio of chloride ions to hydroxide ions, [Cl]/[OH], is a critical factor controlling corrosion initiation [55–57]. Thus, the variation in the hydroxide concentration affects the critical chloride concentration. According to some authors [58–60], a relationship exists between the [Cl]/[OH] ratio and cement content. The variation in cement content can affect the critical chloride concentration. In our case, we did not detect a relationship between cement content and critical chloride concentration, as shown in Fig. 22.

Figure 23 shows the relationship between the chloride concentration and *P*/*C* ratio. The chloride concentration increased with increasing *P*/*C* up to 0.12. When the W/C ratio was greater than 0.12, the chloride concentration decreased. This means that a high proportion of polymer in the repair mortar can reduce the critical chloride concentration by reducing the pH of the pore solution of the material.

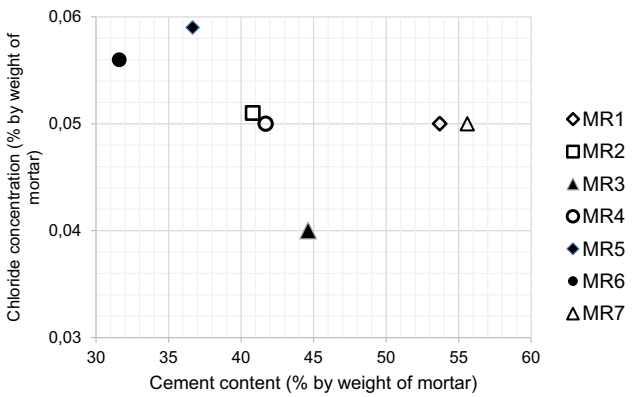

Fig. 22 Relationship between cement fraction and free chloride concentration at a depth of 20 mm (corresponding to cover thickness) at the end of OPC measurements

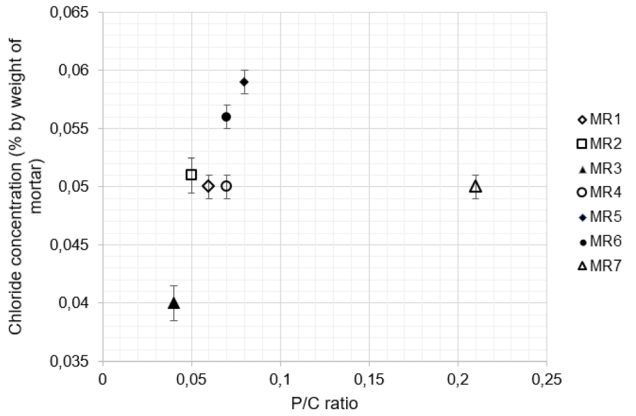

Fig. 23 Relationship between *P*/*C* ratio and free chloride concentration at a depth of 20 mm (corresponding to the cover thickness) at the end of OPC measurements

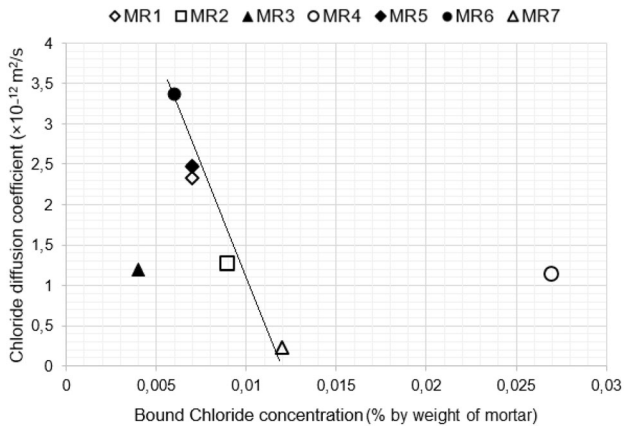

Fig. 24 Relationship between bound chloride at 20 mm (corresponding to the cover thickness) depth and effective diffusion coefficient of chloride

Figure 24 shows the relationship between the bound chlorides (total chloride-free chlorides) and the chloride diffusion coefficient of the mortars. The chloride diffusion coefficient decreased at increased chloride-binding capacities. However, MR2, MR3, and MR4 had almost the same diffusion coefficients, but their chloride-binding capacities were different. This implies that chloride binding is not the only parameter that affects chloride diffusion. Regarding the composition of these materials, increasing the *P*/*C* ratio increased the chloride-binding capacity. Therefore, the *P*/*C* ratio affected the chloride-binding capacity of the mortars.

The critical total chloride concentrations were expressed as a percentage according to the weight of cement (see Fig. 25) for comparison with those available in the literature. Values lie between 0.13 and 0.3% of the mass of cement. These values approach those recommended by the standard EN 206-1, where thresholds are 0.2% for prestressed concrete and 0.4% for reinforced concrete, respectively.

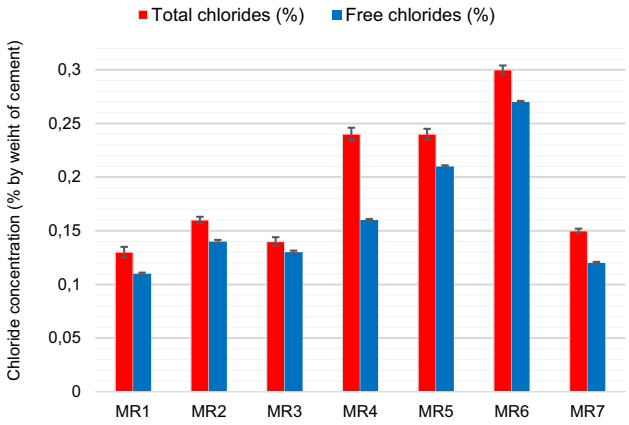

Fig. 25 Critical chloride concentration values at a depth of 20 mm (corresponding to the cover thickness)

4 Conclusion

In this study, the efficiencies of seven repair mortars applied to concrete supports were investigated. The steel protection capacity of the mortars against chloride attack and chloride diffusion along the interface between the concrete support and repair mortar was analysed. The results indicated that the durability parameters (chloride diffusion porosity and pore-size distribution) of the mortars were not sufficient to predict the time evolution of the chloride concentration profiles within the mortar/concrete system. Among the mechanical properties of mortars, the bond strength seems to be a factor that influences chloride penetration. The results also indicate that the polymer content affects the time required to reach a critical chloride concentration. A high proportion of polymers (approximately 20%) decreases chloride diffusivity but also reduces the critical chloride concentration. Future studies should investigate the effect of different polymer dosages on the pH of the pore solution of the mortar and on the critical chloride concentration.

This study showed that mortars MR2, MR3, MR4, and MR7 have good resistance to chloride penetration, and therefore, exhibit a good capacity to protect the reinforcement against corrosion induced by chlorides. Mortars MR1 and MR6 were less effective at protecting the reinforcement against corrosion. Finally, MR5 cannot be applied to marine structures because of its low adhesion to support concrete. The study also showed that the interface can be the weakest part of the chloride diffusion in a repair concrete system.

In addition, based on the results, the following conclusions can be drawn:

- The compressive strength of the mortar with a *P*/*C* ratio of 0.21 was 11 to 22% lower than that of mortar with a *P*/*C* ratio of 4 to 7%.
- A strong relationship exists between the compressive and bond strengths (R^2 = 0.84).
- A high proportion of polymers (*P*/*C* = 0.21) refined the pore-size distribution (main pore diameter in the range of 4 nm).
- A clear decrease (an order of magnitude lower than that of other mortars) in the effective chloride diffusion was observed with the increase in the *P*/*C* ratio to 21%.
- A high-polymer proportion in a mortar (*P*/*C* = 0.2) helps reduce chloride penetration but reduces the critical chloride concentration corresponding to corrosion initiation.
- A bond strength of 0.8 MPa mortar leads to crack development in the mortar/C30 concrete support system and increases the chloride diffusivity, thereby increasing the risk of corrosion initiation.
- A crack width of 5 µm at the interface affects the chloride diffusion along the interface and doubles the chloride diffusion coefficient.
- Critical free chloride concentration values of studied mortars lied between 0.12 and 0.27% according to the mass of cement.

Acknowledgements The authors would like to acknowledge Dr. Egle Conforto from the LaSIE UMR CNRS 7356, La Rochelle University for performing the SEM images.

Declarations

Conflict of Interest No funding was received to assist with the preparation of this manuscript. The authors have no conflict of interests to declare that are relevant to the content of this article.

References

1. Poupard O, Aït-Mokhtar A, Dumargue P (2003) Impedance spectroscopy in reinforced concrete: experimental procedure for monitoring steel corrosion part II: polarization effect. J Mater Sci 38:3521–3526. https://doi.org/10.1023/A:1025600624991
2. Bourbatache K, Millet O, Aït-Mokhtar A (2012) Ionic transfer in charged porous media. Periodic homogenization and parametric study on 2D microstructures. Int J Heat Mass Transf 55:5979–5991. https://doi.org/10.1016/j.ijheatmasstransfer.2012.06.008
3. Aït-Mokhtar A, Poupard O, Dumargue P (2006) Relationship between the transfer properties of the coating and impedance spectroscopy in reinforced cement-based materials. J Mater Sci 41:6006–6014. https://doi.org/10.1007/s10853-006-0493-x
4. Bourbatache K, Millet O, Aït-Mokhtar A, Amiri O (2012) Modeling the chlorides transport in cementitious materials by periodic homogenization. Transp Porous Media 91:437–459. https://doi.org/10.1007/s11242-012-0013-1
5. Soufi A, Mahieux PY, Aït-Mokhtar A, Amiri O (2016) Influence of polymer proportion on transfer properties of repair mortars having equivalent water porosity. Mater Struct 49:383–398. https://doi.org/10.1617/s11527-014-0504-3
6. Zhang X, Du M, Fang H, Shi M, Zhang C, Wang F (2021) Polymer-modified cement mortars: their enhanced properties, applications, prospects, and challenges. Rev Constr Build Mater 299:124290. https://doi.org/10.1016/j.conbuildmat.2021.124290
7. Omikrine Metalssi O, Aït-Mokhtar A (2009) A proposed methodology for a quantitative investigation of carbonation in polymer-modified mortars. Exp Tech 33:59–65. https://doi.org/10.1111/j.1747-1567.2008.00473.x
8. Li G, Zhou Q, Wang W, Lu C, Chen C, Guo Z, Lu C (2023) Chloride diffusion along the interface between concrete matrix and repair materials under flexural loading. Constr Build Mater 372:130829. https://doi.org/10.1016/j.conbuildmat.2023.130829
9. Kim MO (2020) Influence of polymer types on the mechanical properties of polymer-modified cement mortars. Appl Sci 10:1061. https://doi.org/10.3390/app10031061
10. Wang M, Wang R, Zheng S, Farhan S, Yao H, Jiang H (2015) Research on the chemical mechanism in the polyacrylate latex modified cement system. Cem Concr Res 76:62–69. https://doi.org/10.1016/j.cemconres.2015.05.008
11. Eren F, Gödek E, Keskinate M, Tosun Felekog K, Felekoglu B (2017) Effects of latex modification on fresh state consistency, short term strength and long-term transport properties of cement mortars. Constr Build Mater 113:226–233. https://doi.org/10.1016/j.conbuildmat.2016.12.080
12. Mood F, Kashi A, Ramezanianpour A, Pourebrahimi M (2018) Investigation on mechanical and durability properties of polymer and latex-modified concretes. Constr Build Mater 191:144–154. https://doi.org/10.1016/j.conbuildmat.2018.09.198
13. Doğan M, Bideci A (2016) Effect of styrene butadiene copolymer (SBR) admixture on high strength concrete. Constr Build Mater 112:378–385. https://doi.org/10.1016/j.conbuildmat.2016.02.204
14. Qu X, Zhao X (2017) Influence of SBR latex and HPMC on the cement hydration at early age. Case Stud Constr Mater 6:213–218. https://doi.org/10.1016/j.cscm.2017.04.006
15. Gwon S, Jang SY, Shin M (2018) Microstructure evolution and strength development of ultra rapid hardening cement modified with redispersible polymer powder. Constr Build Mater 192:715–730. https://doi.org/10.1016/j.conbuildmat.2018.10.178
16. Li L, Wang R, Lu Q (2018) Influence of polymer latex on the setting time, mechanical properties and durability of calcium sulfoaluminate cement mortar. Constr Build Mater 169:911–922. https://doi.org/10.1016/j.conbuildmat.2018.03.005
17. Tran NP, Nguyen TN, Ngo TD (2022) The role of organic polymer modifiers in cementitious systems towards durable and resilient infrastructures: a systematic review. Constr Build Mater 360:129562. https://doi.org/10.1016/j.conbuildmat.2022.129562
18. Liu Q, Liu R, Wang Q, Liang R, Li Z, Sun G (2021) Cement mortar with enhanced flexural strength and durability-related properties using in situ polymerized interpenetration network. Front Struct Civ Eng 15:99–108. https://doi.org/10.1007/s11709-021-0721-0
19. Li X, Liu R, Li S, Zhang C, Li J, Cheng B, Liu Y, Ma C, Yan J (2022) Effect of SBR and XSBRL on water demand, mechanical strength and microstructure of cement paste. Constr Build Mater 332:127309. https://doi.org/10.1016/j.conbuildmat.2022.127309
20. Zhang H, Kong X, Lu Z, Jansen D, Pakusch J, Wang S (2019) Pore structure of hardened cement paste containing colloidal polymers with varied glass transition temperature and surface charges. Cement Concr Compos 95:154–168. https://doi.org/10.1016/j.cemconcomp.2018.11.001

21. Aggarwal LK, Thapliyal PC, Karade SR (2007) Properties of polymer modified mortars using epoxy and acrylic emulsions. Constr Build Mater 21:379–383. https://doi.org/10.1016/j.conbuildmat.2005.08.007
22. Saija LM (1995) Waterproofing of Portland cement mortars with a specially designed polyacrylic latex. Cem Concr Res 25:503–509. https://doi.org/10.1016/0008-8846(95)00039-F
23. Zhong S, Chen Z (2002) Properties of latex blends and its modified cement mortars. Cem Concr Res 32:1515–1524. https://doi.org/10.1016/S0008-8846(02)00813-X
24. Gao JM, Qian CX, Wang B, Morino K (2002) Experimental study on properties of polymer-modified cement mortars with silica fume. Cem Concr Res 32:41–45. https://doi.org/10.1016/S0008-8846(01)00626-3
25. Yang Z, Shi X, Creighton AT, Peterson MM (2009) Effect of styrenebutadiene rubber latex on the chloride permeability and microstructure of portland cement mortar. Constr Build Mater 23:2283–2290. https://doi.org/10.1016/j.conbuildmat.2008.11.011
26. Rashid K, Ueda T, Zhang D, Miyaguchi K, Nakai H (2015) Experimental and analytical investigations on the behavior of interface between concrete and polymer cement mortar under hygrothermal conditions. Constr Build Mater 94:414–425. https://doi.org/10.1016/j.conbuildmat.2015.07.035
27. Assaad J, Daou Y (2017) Behavior of structural polymer-modified concrete containing recycled aggregates. J Adhes Sci Technol 31:874–896. https://doi.org/10.1080/01694243.2016.1235750
28. Assaad JJ (2018) Development and use of polymer-modified cement for adhesive and repair applications. Constr Build Mater 163:139–148. https://doi.org/10.1016/j.conbuildmat.2017.12.103
29. Jo YK (2020) Adhesion in tension of polymer cement mortar by curing conditions using polymer dispersions as cement modifier. Constr Build Mater 242:118134. https://doi.org/10.1016/j.conbuildmat.2020.118134
30. Abdulrahman PI, Bzeni PI (2022) Bond strength evaluation of polymer modified cement mortar incorporated with polypropylene fibers. Case Stud Constr Mater 17:e01387. https://doi.org/10.1016/j.cscm.2022.e01387
31. EN 1504 (2005) Products and systems for the protection and repair of concrete structures. The European Standards.
32. NF EN 206–1. (2002) Concrete, part 1: specification, performance, production and conformity, The European Standards
33. EN 12190 (1998) Products and systems for the protection and repair of concrete structures. Test methods: determination of compressive strength for repair mortars. The European Standards.
34. EN 196–1 (2006) Cement test methods Part 1: Determination of mechanical strengths. The European Standards.
35. NF EN 13412 (2006). Products and systems for protecting and repairing concrete structures - Test methods - Determination of the modulus of elasticity in compression. The European Standards.
36. NF EN 1542 (1999) Products and systems for protecting and repairing concrete structures - Test methods - Direct traction adhesion measurement. The European Standards
37. NF EN 12390–3 (2019) Tests for hardened concrete - Part 3: compressive strength of specimens
38. NF EN 12390–6 (2012). Tests for hardened concrete - Part 6: determination of tensile strength by splitting test specimens
39. NF EN 12390–13 (2021). Tests for hardened concrete - Part 13: determination of the secant modulus of elasticity in compression
40. Arliguie G, Hornain H (2007) GranDuBé, grandeurs associées à la durabilité des bétons, France
41. Aït-Mokhtar A, Amiri O, Dumargue P, Bouguerra A (2004) On the applicability of Washburn law: study of mercury and water flow properties in cement-based materials. Mater Struct 37:107–113. https://doi.org/10.1007/BF02486606
42. ASTM C876–09 (1991) Standard Test Method for Corrosion Potentials of Uncoated Reinforcing Steel in Concrete
43. Medeiros MHF, Helene P, Selmo S (2009) Influence of EVA and acrylate polymers on some mechanical properties of cementitious repair mortars. Constr Build Mater 23:2527–2533. https://doi.org/10.1016/j.conbuildmat.2009.02.021
44. Tian Y, Jin XY, Jin NG, Zhao R, Li ZJ, Ma HY (2013) Research on the microstructure formation of polyacrylate latex modified mortars. Constr Build Mater 47:1381–1394. https://doi.org/10.1016/j.conbuildmat.2013.06.016
45. Gholinezhad F, Moghbeli MR, Aghaei A, Allahverdi A (2021) Effect of organoclay reinforced acrylate latex particles on the cement paste performance. J Dispersion Sci Technol 42:416–431. https://doi.org/10.1080/01932691.2019.1699425
46. Eren F, Gödek E, Keskinate M, Tosun-Felekog K, Felekoglu B (2017) Effects of latex modification on fresh state consistency, short term strength and long-term transport properties of cement mortars. Constr Build Mater 113:226–233. https://doi.org/10.1016/j.conbuildmat.2016.12.080
47. Hemkemeiera TA, Almeida FCR, Salesa A, Klemm AJ (2022) Corrosion monitoring by open circuit potential in steel reinforcements embedded in cementitious composites with industrial wastes. Case Stud Constr Mater 16:e01042. https://doi.org/10.1016/j.cscm.2022.e01042
48. Nguyen QD, Castel A (2020) Reinforcement corrosion in limestone flash calcined clay cement-based. Cement Concr Res 132:106051. https://doi.org/10.1016/j.cemconres.2020.106051
49. Aattache A, Soltan R (2020) Durability-related properties of early-age and long-term resistant laboratory elaborated polymer-based repair mortars. Constr Build Mater 235:117494. https://doi.org/10.1016/j.conbuildmat.2019.117494
50. Emmons PH, Vaysburd AM (1996) System concept in design and construction of durable concrete repairs. Constr Build Mater 10:69–75. https://doi.org/10.1016/0950-0618(95)00065-8
51. Morgan DR (1996) Compatibility of concrete repair materials systems. Constr Build Mater 10:57–67. https://doi.org/10.1016/0950-0618(95)00060-7
52. Gouda VK (2013) Corrosion and corrosion inhibition of reinforcing steel immersed in alkaline solutions. Br Corros J 5:198–203. https://doi.org/10.1179/000705970798324450
53. Glass GK, Buenfeld NR (1997) The presentation of the chloride threshold level for corrosion of steel in concrete. Corros Sci 39:1001–1013. https://doi.org/10.1016/S0010-938X(97)00009-7
54. Goni S, Andrade C (1990) Synthetic concrete pore solution chemistry and rebar corrosion rate in the presence of chlorides. Cem Concr Res 20:525–539. https://doi.org/10.1016/0008-8846(90)90097-H
55. Page CL, Lambert P, Vassie PRW (1991) Investigations of reinforcement corrosion. 1. The pore electrolyte phase in chloride-contaminated concrete. Mater Struct 24:243–252. https://doi.org/10.1007/BF02472078
56. Hussain SE, Al-Musallam A, Al-Gahtani AS (1995) Factors affecting threshold chloride for reinforcement corrosion in concrete. Cem Concr Res 25:1543–1555. https://doi.org/10.1016/0008-8846(95)00148-6
57. Thomas M (1996) Chloride thresholds in marine concrete. Cem Concr Res 26:513–519. https://doi.org/10.1016/0008-8846(96)00035-X

58. Bamforth PB (1999) The derivation of input data for modelling chloride ingress from eight-years UK coastal exposure trials. Mag Concr Res 51:87–96. https://doi.org/10.1680/macr.1999.51.2.87
59. Alonso C, Castellote M, Andrade C (2022) Chloride threshold dependence of pitting potential of reinforcements. Electrochem Acta 47:3469–3481. https://doi.org/10.1016/S0013-4686(02)00283-9
60. Oh BH, Jang SY, Shin YS (2003) Experimental investigation of the threshold chloride concentration for corrosion initiation in reinforced concrete structures. Mag Concr Res 55:117–124. https://doi.org/10.1680/macr.2003.55.2.117